Predicted Temperature Field in a Thermomechanically Heated Viscoplastic Space Truss Structure

D.H. Allen* and W.E. Haisler†
Texas A&M University, College Station, Texas

This paper focuses on the effect of thermomechanically induced heating on the response of a single member of a space truss structure that behaves viscoplastically. The governing equations are given for a typical truss member, in which material inelasticity is reflected in constitutive equations via a set of internal state variables, each characterized by a history-dependent growth law. The governing equations are coupled in the sense that temperature and displacement are dependent on each other. This difficulty, together with the fact that the inelastic constitutive equations are nonlinear and numerically stiff, requires that a computationally complex semidiscretized finite element spatial technique be utilized to obtain a solution. This procedure is utilized to predict the response of a typical metallic space truss member under vibrational or cyclic loading. Particular interest is placed on the temperature rise in such a member due to hysteretic loss during structural vibrations and in the presence of complex thermal boundary conditions. Example cases are constructed for a typical cylindrical bar of 5086 aluminum, both with and without special coatings. Results indicate that significant, possibly even catastrophic, heating can occur due to thermomechanical coupling.

Nomenclature

A	= cross-sectional area
c	= absorbing portion of perimeter of an element normal to longitudinal axis
C_v	= specific heat at constant elastic strain
$D_0, n, m, Z_1, Z_I, Z_0, r$	= material constants used in Bodner and Partom's model[1]
E	= Young's modulus in the axial coordinate direction
F_E	= Earth radiation view factor
k	= coefficient of axial thermal conductivity
L	= length of the structural element
P	= axial internal resultant force
p_x	= axial externally applied force per unit length
$\mathbf{q}$	= heat flux vector
q	= axial component of heat flux
q_c	= flux on longitudinal boundary
q_E, q_s	= earth and solar radiation flux, respectively
r	= internal heat source per unit mass
s	= surface area
S_c	= area of the longitudinal surface of the bar
t	= time
T	= temperature
T_D	= deep space temperature
T_E	= equilibrium temperature of structural component
T_R	= reference temperature at which no deformation is observed at zero load
T_x	= end traction in units of force per unit area
u	= axial displacement component
v, w	= test functions
x	= axial coordinate dimension
α	= coefficient of thermal expansion in the axial coordinate direction
α_1, α_2	= internal state variables representing axial inelastic strain and drag stress, respectively
α_s	= absorptivity
ε	= axial strain component
λ_E, λ_s	= incident angle of Earth and solar radiation, respectively, on structural component
ρ	= mass density
σ	= axial stress component
σ_s	= Stefan-Boltzmann constant = 5.775×10^{-11} MPa m/s/(K)^4

Introduction

IT is well known that in viscoplastic metals a certain amount of mechanical energy is converted to heat, thus resulting in a temperature rise in the medium. In recent research[2,3] a model has been developed for predicting this effect by utilizing thermodynamic constraints together with constitutive equations of the internal state variable type.[4] Furthermore, it has been shown that in a perfectly insulated uniaxial bar,[3] as well as in a uniaxial bar with insulated longitudinal surface and fixed end temperature,[5] significant temperature rise can occur in the component during cyclic loading.

Due to microgravity, large space structures will require control of flexible body modal response. One possible mechanism for incorporating passive control is to design selected members in the structure to operate inelastically. The conversion of hysteretic strain energy loss to heat will result in mechanical damping of the structure. The purpose of the current research is to simulate the response of a typical metallic space truss structural element (see Fig. 1) in the postyielded state and to determine if significant heating occurs when this component is subjected to cyclic mechanical loading. The factors of interest in this simulation are the effects of thermal boundary conditions and loading rate on the thermal response. In particular, it is of interest to determine if radiative boundary conditions on the longitudinal surface of the truss component are significant enough to carry off all heat generated due to hysteretic loss.

The paper first reviews the governing field equations, then briefly discusses the procedure whereby a numerical algorithm is constructed for modeling the problem. This is followed by a

Submitted Feb. 5, 1985; presented as Paper 85-0829 at the AIAA/ASME/ASCE/AHS 26th Structures, Structural Dynamics and Materials Conference, Orlando, FL, April 15-17, 1985; revision received July 18, 1985.

*Associate Professor, Aerospace Engineering. Member AIAA.
†Professor and Head, Aerospace Engineering. Associate Fellow AIAA.

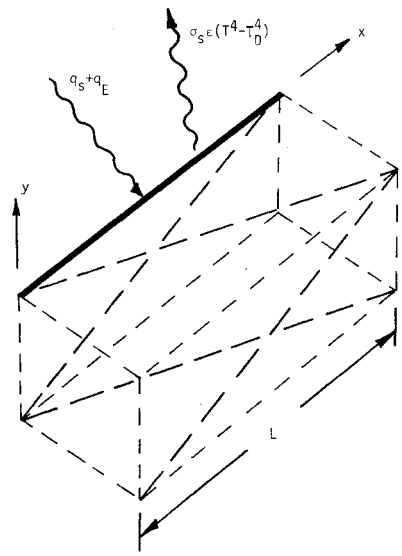

Fig. 1 Typical space truss structural element.

detailed discussion of the implementation of thermal boundary conditions. Finally, example results are obtained for representative space structural components.

Governing Field Equations

The governing field equations were presented in Ref. 5 for quasistatic conditions. For problems involving inertial effects, the governing equations are as follows:

1) Equilibrium,[6]

$$\frac{\partial P}{\partial x} = p_x(x) \tag{1}$$

where the axial resultant P is defined by

$$P = \int \sigma \, dA \tag{2}$$

and

$$p_x \equiv \int_{S_c} T_x \, ds \tag{3}$$

2) Strain-displacement relation

$$\varepsilon = \frac{\partial u}{\partial x} \tag{4}$$

3) Thermomechanical constitution,

$$\sigma = E[\varepsilon - \alpha_1 - \alpha(T - T_R)] \tag{5}$$

$$\dot{\alpha}_1 = \frac{2}{\sqrt{3}} D_0 \frac{\sigma}{|\sigma|} \exp\left[-\left(\frac{n+1}{2n} \right) \left(\frac{\alpha_2}{\sigma} \right)^{2n} \right] \tag{6}$$

$$\dot{\alpha}_2 = m(Z_1 - \alpha_2)\sigma\dot{\alpha}_1 - A_1 Z_1 \left(\frac{\alpha_2 - Z_I}{Z_1} \right)^r \tag{7}$$

$$q = -k \frac{\partial T}{\partial x} \tag{8}$$

where α_1 and α_2 are the internal state variables (ISV) representing inelastic strain and drag stress, respectively, in the constitutive model developed by Bodner and Partom.[1] This model has been shown to be accurate for a variety of materials under uniaxial cyclic loading conditions,[7,8] including aluminum at room temperature.[9] Several other constitutive models have been developed for viscoplastic metals, and these are reviewed in Refs. 7, 9, and 10. Finally,

4) Conservation of energy,[3,5]

$$\left[(E\varepsilon - E\alpha_1 + E\alpha T_R) \frac{\partial \alpha_1}{\partial t} + E\alpha^2 T \frac{\partial T}{\partial t} \right] - E\alpha T \frac{\partial \varepsilon}{\partial t} - \rho C_v \frac{\partial T}{\partial t} - \frac{\partial q}{\partial x} + \rho r = 0 \tag{9}$$

Conservation of mass is satisfied trivially (under the assumption of small motions in a closed system), and the second law of thermodynamics has been previously shown to be satisfied by the above equations.[2,4]

The governing equations are adjoined with appropriate initial and boundary conditions[5] such that a well-posed boundary value problem is constructed in terms of the following dependent variables, which are sought as functions of x and t: $\sigma, \varepsilon, u, q, T, P, \alpha_1$, and α_2. Due to ISV growth laws (6) and (7), as well as radiative boundary conditions, the problem is nonlinear.

Solution Procedure

As described in detail in Ref. 5 for the quasistatic problem, the solution is obtained using the semidiscretized finite element technique, in which finite elements are constructed spatially and finite differencing is used in time. The result is a time-marching algorithm, which is reviewed here briefly.

First, Eqs. (4) and (5) are substituted into Eq. (2); this result is substituted into Eq. (1) to give the following equilibrium equation:

$$\frac{\partial}{\partial x} \left\{ EA \left[\frac{\partial u}{\partial x} - \alpha_1 - \alpha(T - T_R) \right] \right\} = -p_x(x) \tag{10}$$

Next, Eq. (4) is substituted into Eq. (9) to obtain the coupled energy balance law

$$\left[\left(E\frac{\partial u}{\partial x} - E\alpha_1 + E\alpha T_R \right) \frac{\partial \alpha_1}{\partial t} + E\alpha^2 T \frac{\partial T}{\partial t} \right] - E\alpha T \frac{\partial^2 u}{\partial t \, \partial x} - \rho C_v \frac{\partial T}{\partial t} - \nabla \cdot \mathbf{q} + \rho r = 0 \tag{11}$$

The result is a set of two coupled partial differential equations in terms of axial displacement $u = u(x, t)$ and temperature $T = T(x, t)$.

Variational Principles and Finite Element Discretization

Selecting a suitably smooth test function $v = v(x)$ over the domain of some element Ω_e, $x_e < x < x_{e+1}$, one may construct the following variational principle from Eq. (10):[11]

$$-\int_{x_e}^{x_{e+1}} EA \frac{\partial v}{\partial x} \left[\frac{\partial u}{\partial x} - \alpha_1 - \alpha(T - T_R) \right] dx = -v(x_{e+1}) P(x_{e+1}) + v(x_e) P(x_e) - \int_{x_e}^{x_{e+1}} v p_x \, dx \tag{12}$$

where the boundary terms result from the standard integration by parts.

The variational principle for heat equation (11) is constructed by first integrating this equation against a test function $w = w(x)$ on Ω_e to obtain

$$\int_{\Omega_e} w \left\{ \left[(E\varepsilon - E\alpha_1 + E\alpha T_R) \frac{\partial \alpha_1}{\partial t} + E\alpha^2 T \frac{\partial T}{\partial t} \right] - E\alpha T \frac{\partial^2 u}{\partial x \, \partial t} - \rho C_v \frac{\partial T}{\partial t} + \nabla \cdot \mathbf{q} + \rho r \right\} dV = 0 \tag{13}$$

Integrating the flux term by parts, assuming that nonaxial components of flux are negligible, and substituting Eq. (8) will thus result in

$$\int_{x_e}^{x_{e+1}} w\left\{ A\left[\left(E\frac{\partial u}{\partial x} - E\alpha_1 + E\alpha T_R\right)\frac{\partial \alpha_1}{\partial t} + E\alpha^2 T\frac{\partial T}{\partial t}\right] - AE\alpha T\frac{\partial^2 u}{\partial t\,\partial x} - A\rho C_v\frac{\partial T}{\partial t} - kA\frac{\partial w}{\partial x}\frac{\partial T}{\partial x}\right\} \mathrm{d}x$$
$$= -w(x_{e+1})Aq(x_{e+1}) + w(x_e)Aq(x_e) - \int_{x_e}^{x_{e+1}} cwq_c\,\mathrm{d}x + \int_{x_e}^{x_{e+1}} wA\left(\rho C_v\frac{\partial T}{\partial t} - \rho r\right)\mathrm{d}x \qquad (14)$$

Variational Eqs. (12) and (14) are now discretized by assuming the following displacement and temperature fields in a typical element (superscripted e):

$$u(x,t) = \sum_{i=1}^{3} u_i^e(t)\psi_i^e(x) \quad x_e < x < x_{e+1} \qquad (15)$$

$$T(x,t) = \sum_{i=1}^{2} T_i^e(t)\phi_i^e(x) \quad x_e < x < x_{e+1} \qquad (16)$$

where u_i^e and T_i^e are nodal displacements and temperatures, respectively, and ψ_i^e and ϕ_i^e are quadratic and linear shape functions, respectively.[11] Furthermore, v and w are endowed with the properties of u and T. Note that a higher-order element must be used for displacement than temperature due to the fact that temperature produces strain rather than displacement.

Timewise discretization is implemented via the following backward finite difference equations:

$$\frac{dT_m^e}{dt}(t) \cong \left[T_m^e(t) - T_m^e(t-\Delta t)\right]/\Delta t \quad m = 1,2 \qquad (17)$$

$$\frac{du_m^e}{dt}(t) \cong \left[u_m^e(t) - u_m^e(t-\Delta t)\right]/\Delta t \quad m = 1,2,3 \qquad (18)$$

The above equations require small time steps in order to guarantee numerical accuracy. However, they are unconditionally stable, which is necessary because ISV growth laws (6) and (7) are numerically stiff.[12]

Substitution of Eqs. (15) through (18) into the governing field equations in variational form will result in the following algebraic equations:

$$\left[\begin{array}{c|c} 3\times 3 & 3\times 2 \\ K^e & S^e \\ \hline \bar{\bar{K}}^e & \bar{\bar{S}}^e \end{array}\right]\left\{\begin{array}{c} U^e \\ \hline T^e \end{array}\right\} = \left\{\begin{array}{c} F^e \\ \hline \bar{F}'^e \end{array}\right\} \qquad (19)$$

$$\underbrace{2\times 3 \quad 2\times 2}_{5\times 5} \quad 5\times 1 \quad 5\times 1$$

where $[K^e]$, $[S^e]$, $[\bar{\bar{K}}^e]$, $\bar{\bar{S}}^e]$, and $\{F^e\}$ are as described in Ref. 5, and

$$\bar{F}_i'^e \equiv \bar{F}_i^e - \int_{x_e}^{x_{e+1}} c\phi_i^e q_c\,\mathrm{d}x \qquad (20)$$

where $\bar{F}_i^e$ is as defined in Ref. 5. The last term in the above equation accounts for thermal flux boundary conditions on the longitudinal surface of an element.

After global assembly and imposition of boundary conditions Eqs. (19) can be solved in a time-marching scheme in order to obtain the nodal displacements and temperatures as functions of time.

Global assembly of the element equations is accomplished in the standard way using the Boolean matrix.[11]

Imposition of Boundary Conditions

For a typical space truss structural element, the boundary conditions are assumed to be of the following type:

$$u(0,t) = u_t^0 = \text{known}$$
$$u(L,t) = u_t^L = \text{known}$$
$$T(0,t) = T_t^0 = \text{known}$$
$$T(L,t) = T_t^L = \text{known} \qquad (21)$$

and[13]

$$q_c = -\alpha_s\left[q_s\cos\lambda_s + F_E(1-\alpha_E)q_s\cos\lambda_e + F_E q_E\cos\lambda_e\right] + \sigma_s\varepsilon\left(T^4 - T_D^4\right) \qquad (22)$$

where the first term is the solar radiation flux absorbed by the body, the second the solar radiation flux reflected by the Earth and absorbed by the body, the third the Earth radiation flux absorbed by the body, and the last the flux radiated by the member to space.

The above boundary conditions may be implemented to the discretized global equations in the standard way.[11] Although Eq. (22) technically includes the unknown temperature field, the component temperature is treated as a known quantity in this term for each time step. This approximation is acceptable due to the fact that the numerical stiffness of constitutive Eqs. (6) and (7) requires extremely small time steps in order to obtain an accurate solution.

Example Problems

A typical structural element has been modeled with properties shown in Table 1. The material properties were obtained experimentally in the Texas A&M Mechanics and Materials Center[9] for Al 5086 at room temperature, which is similar to Al 6061-T6.

Sample cases were constructed for various cyclic loading rates for two different sets of thermal boundary conditions, as described in Table 2. Both cases are considered to be worst cases in that the component is in a maximum radiation flux condition at the maximum equilibrium temperature during one orbital cycle. The two cases differ in the emissivity and absorptivity values for the component due to differences in surface treatment of the component. For case I the component is anodized, and for case II the component is painted with high emissivity IITRE-S13GLO white paint.[14]

We now consider two elements in a large space structure (see Fig. 1). Both elements are constructed of the same material and are geometrically identical. However, element 1 is painted with the high emissivity paint described above and is in full view of both Earth and sun, whereas element 2 is anodized and is in view of Earth only. For this case, as described in Table 2, the components have identical equilibrium temperatures $T_E = 295$ K [obtained by setting $q_c = 0$ in Eq. (22)].

In both cases the structural members have been subjected to 50 cycles of loading at three different frequencies: 1, 5, and 25 Hz. These frequencies have been selected as representative of resonant frequencies in a representative space structure. For example, a typical structure analyzed in Ref. 15 has resonant frequencies of 4.1 Hz and 3.4 Hz in the first two modes. Because the resonant frequency of the first mode in the structural element itself is 240 Hz, inertial effects may be neglected in these examples.

Results for the cases described above are shown in Figs. 2-8. In Figs. 2-4 the cyclic stress-strain curve is shown at the location $x = L/2$ for case I and at all three loading rates. It is found that in all cases the specimen reaches cyclic saturation after approximately 5 cycles. Thereafter, the hysteretic energy loss per cycle becomes a constant value.

Table 1 Material and geometric properties for a typical truss structural element (from Ref. 14)

$C_v = 900$ J/kg/K (0.215 Btu/lb/°F)
$\alpha = 23.8 \times 10^{-6}$ in./in./K (13.2×10^{6} in./in./°F)
$k = 1.27 \times 10^{-4}$ MPa m^2/s/K (73.4 Btu/ft/h/°F)
$E = 71.0 \times 10^{3}$ MPa (10.3×10^{6} psi)
$A = 6.45 \times 10^{-4}$ m^2 (1.00 in.^{2})
$T_R = 295$ K (72°F)
$L = 3.66$ m (12.0 ft)
$D_0 = 10 \times 10^{3}$ m/m
$A_1 = 1.685 \times 10^{-7}$ s^{-1}
$n = 2.355$
$m = 0.1770$ MPa^{-1} (1.2205 ksi^{-1})
$Z_1 = 620.1$ MPa (89.93 ksi)
$Z_I = 0$
$r = 0$
$\rho = 2.66$ Mg/m^3 (0.096 lb/in.^{3})
$c = 0.0508$ m (0.8333 ft)
$Z_0 = 387.8$ MPa (56.25 ksi)

Table 2 Thermal properties for example cases I and II (from Refs. 13 and 14)

	Case I	Case II
α_s	0.20 (degraded)	0.3218 (degraded)
ε	0.85	0.24
λ_s	0°	0°
q_s	1.39 MPa m/s	0
q_E	0.20 MPa m/s	0.20 MPa m/s (4080 km altitude)
λ_e	0°	0°
T_D	0 K	0 K
α_E	0.30	0.30
F_E	0.4	0.4
T_{EQ}	296.2 K (73.6°F)	296.2 K

CASE I: Surface painted with S13GLO white
CASE II: Chromic anodized surface

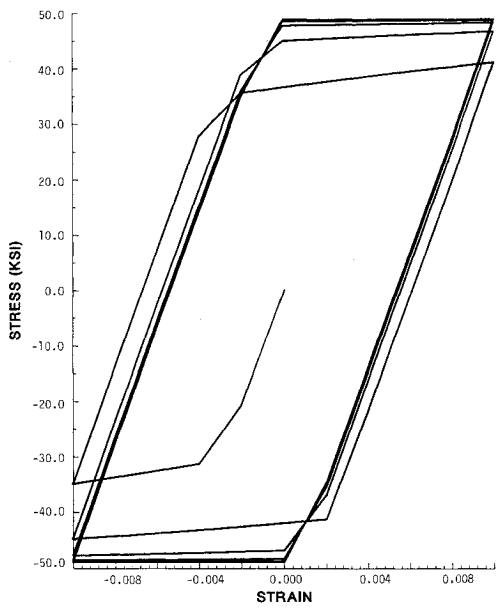

Fig. 2 Cyclic stress-strain curve at $x = L/2$ for case I coating loaded at 1 Hz.

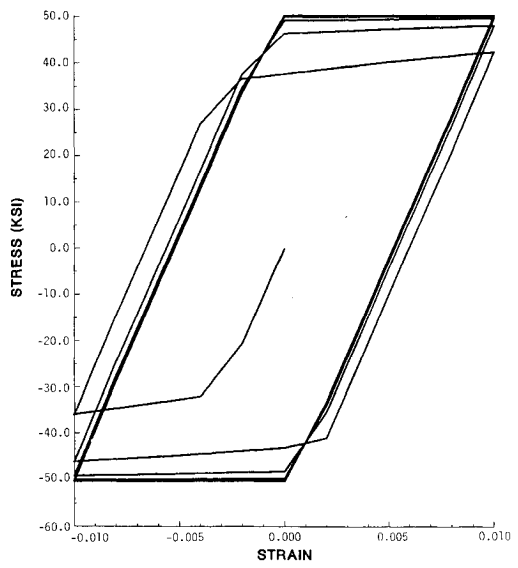

Fig. 3 Cyclic stress-strain curve at $x = L/2$ for case I coating loaded at 5 Hz.

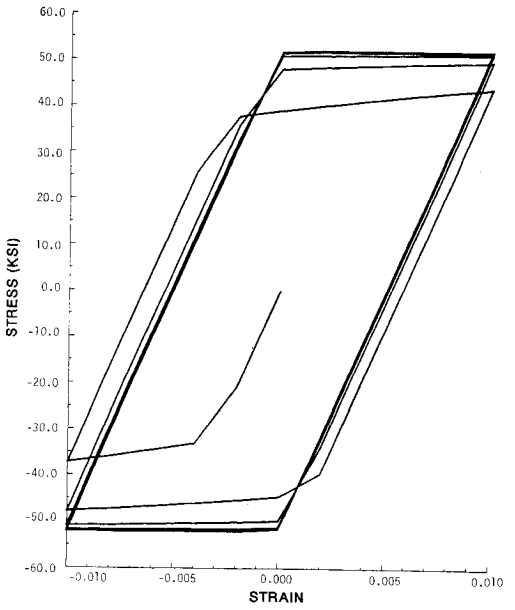

Fig. 4 Cyclic stress-strain curve at $x = L/2$ for case I coating loaded at 25 Hz.

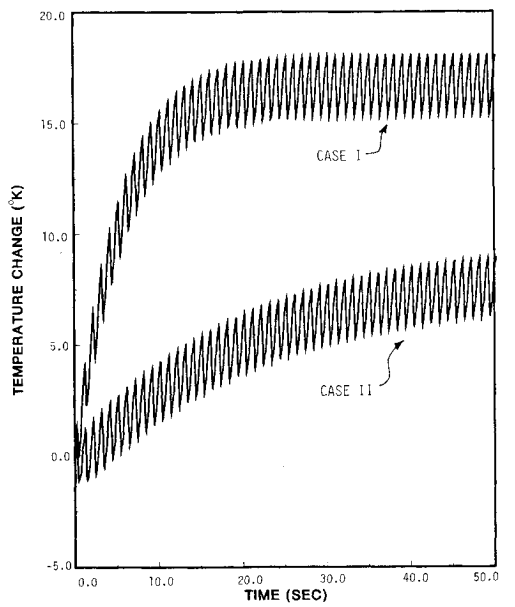

Fig. 5 Temperature vs time curves at $x = L/2$ for loading at 1 Hz.

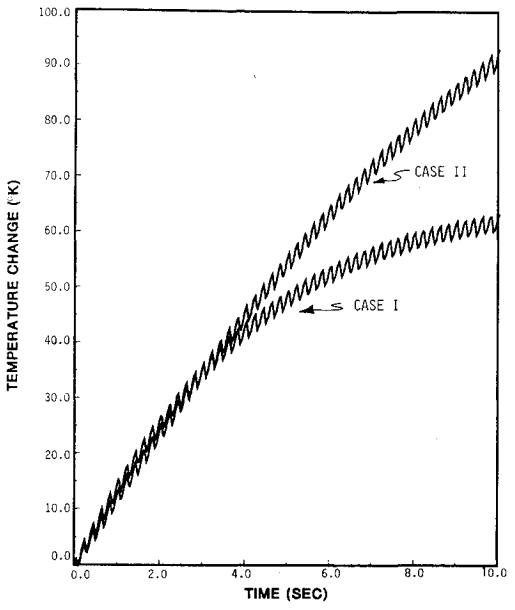

Fig. 6 Temperature vs time curves at $x = L/2$ for loading at 5 Hz.

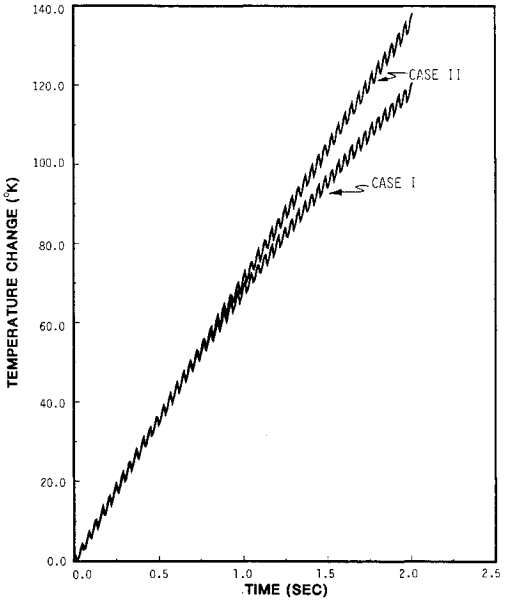

Fig. 7 Temperature vs time curves at $x = L/2$ for loading at 25 Hz.

In Figs. 5-7 the temperature rise is plotted for both cases at all three loading rates. As expected, the amount of temperature rise increases dramatically with loading rate. For example, after 50 cycles the total temperature rise at $x = L/2$ is 17.5 K (1 Hz), 62.5 K (5 Hz), and 119.7 K (25 Hz) for case I. Furthermore, it is apparent that, while neither surface treatment can be regarded as resulting in negligible heating, at the higher loading rates the anodized surface treatment produces temperature rises significantly higher than those produced by painting with IITRE-S13GLO paint. Finally, these authors believe that the nonlinear nature of the average temperature rise per cycle suggests that the temperature rise asymptotically approaches some upper bound, although this belief cannot be corroborated at this time due to the large computer times required in the current algorithm.

Figure 8 shows that the spatial temperature variation at 5 Hz is approximately spatially homogeneous. Apparently, a very thin boundary layer forms near the end of the component, and this boundary layer has little effect on the temperature at $x = L/2$. In fact, subsequent investigations by the authors have shown that, at least for the geometry and physical conditions considered herein, identical results may be obtained more efficiently by neglecting spatial variations in displacement and temperature.

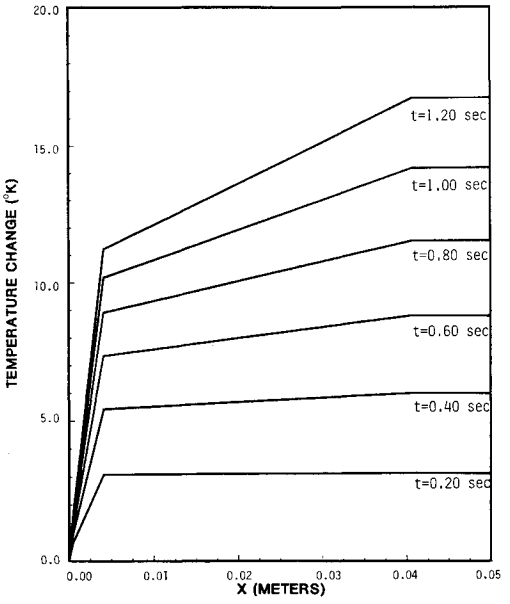

Fig. 8 Spatial temperature variation for case I coating loaded at 5 Hz.

Conclusion

The current research has attempted to predict the response of a typical space structural element that is viscoplastic and is subjected to various cyclic loading conditions in the presence of radiation boundary conditions. Several general conclusions can be made as a result of this research:

1) Significant temperature rises may occur due to hysteretic loss, although the precise amount depends on loading rate and surface treatment.

2) The special paint IITRE-S13GLO appears to produce significantly lower temperature rises than anodized surface treatment.

3) The temperature rise appears to be approaching an upper bound that is dependent on loading rate and surface treatment.

4) The thermal boundary layer that forms near the end of the member appears to have little effect on the far-field temperature rise.

These conclusions indicate that future research on this subject should perhaps concentrate on spatial variations in the radial direction rather than the axial direction. More importantly, these results indicate that an inelastic structural component may undergo temperature rises during structural vibrations that are so substantial that the material properties of the component may be further degraded, thus leading to failure of the component and perhaps of the entire structure.

Acknowledgments

The authors wish to thank Dr. M.S. Pilant for his interesting discussions and helpful advice on this research. Support was provided by the Air Force Office of Scientific Research under Contract F49620-83-C-0067.

References

[1] Bodner, S.R. and Partom, Y., "Constitutive Equations for Elastic-Viscoplastic Strain-Hardening Materials," *Journal of Applied Mechanics*, Vol. 42, 1975, pp. 385-389.

[2]Allen, D.H., "Thermodynamic Constraints on the Constitution of a Class of Thermoviscoplastic Solids," Texas A&M University Mechanics and Materials Center, College Station, MM 12415-82-10, Dec. 1982.

[3]Allen, D.H., "A Prediction of Heat Generation in a Thermoviscoplastic Uniaxial Bar," *International Journal of Solids Structures*, Vol. 21, 1985, pp. 325-342.

[4]Coleman, B.D. and Gurtin, M.E., "Thermodynamics with Internal State Variables," *Journal of Chemical Physics*, Vol. 47, 1967, pp. 597-613.

[5]Allen, D.H., "Predicted Axial Temperature Gradient in a Viscoplastic Uniaxial Bar Due to Thermomechanical Coupling," Texas A&M University Mechanics and Materials Center, College Station, MM 4875-84-15, Nov. 1984 (to appear in *International Journal for Numerical Methods in Engineering*, 1986).

[6]Allen, D.H. and Haisler, W.E., *Introduction to Aerospace Structural Analysis*, John Wiley & Sons, New York, 1985.

[7]Milly, T.M. and Allen, D.H., "A Comparative Study of Nonlinear Rate-Dependent Mechanical Constitutive Theories for Crystalline Solids at Elevated Temperatures," Virginia Polytechnic Institute and State University, Blacksburg, VPI-E-82-5, March 1982.

[8]Bodner, S.R., "Review of a Unified Elastic-Viscoplastic Theory," The Technion, Haifa, Israel, AFOSR-84-0042, 1984.

[9]Beek, J.M., "A Comparison of Current Models for Nonlinear Rate-Dependent Material Behavior of Crystalline Solids," Thesis, Texas A&M University, May, 1986.

[10]Allen, D.H. and Beek, J.M., "On the Use of Internal State Variables in Thermoviscoplastic Constitutive Equations," *Proceedings of the 2nd Symposium on Nonlinear Constitutive Relations for High Temperature Applications*, June 1984.

[11]Reddy, J.N., *An Introduction to the Finite Element Method*, McGraw-Hill Book Co., New York, 1984.

[12]Gear, C.W., "The Automatic Integration of Stiff Ordinary Differential Equations," *Information Processing 68*, North Holland, The Netherlands, Vol. 1, 1968, p. 187.

[13]Brogren, E.W., Barclay, D.L., and Straayer, J.W., "Simplified Thermal Estimation Techniques for Large Space Structures," NASA-CR-145253, Oct. 1977.

[14]"Long Duration Exposure Facility (LDEF) Experimenter Users Handbook," NASA Langley Research Center, LDEF 840-2, 1978.

[15]Kalyanasundaram, S., Lutz, J.D., Haisler, W.E., and Allen, D.H., "Effect of Degradation of Material Properties on the Dynamic Response of Large Space Structures," *Proceedings of the AIAA/ASME/ASCE/AHS 26th Structures, Structural Dynamics and Materials Conference, Orlando, Florida*, Pt. 2, April 1985, pp. 545-551.